# New diterpenes from *Salvia pseudorosmarinus* and their activity as inhibitors of monoacylglycerol lipase (MAGL)

Marinella De Leo[a,d], Conny Guillen Huallpa[a], Britt Alvarado[b], Carlotta Granchi[a], Giulio Poli[a], Nunziatina De Tommasi[c,*], Alessandra Braca[a,d]

[a]*Dipartimento di Farmacia, Università di Pisa, Via Bonanno 33, 56126, Pisa, Italy*

[b]*Facultad de Farmacia y Bioquímica, Universidad Nacional Mayor de San Marcos, CIRNA, NATURE Jardín Botánico, Jr. Puno 1002, Lima, Peru*

[c]*Dipartimento di Farmacia, Università di Salerno, Via Giovanni Paolo II, 84084 Fisciano (SA), Italy*

[d]*Centro Interdipartimentale di Ricerca "Nutraceutica e Alimentazione per la Salute", Università di Pisa, via del Borghetto 80, 56124 Pisa, Italy*

* Corresponding author. Tel.: +39 089 969754; fax: +39 089 969602.

*E-mail address*: detommasi@unisa.it (N. De Tommasi).

**Abstract**

As a part of our ongoing research program on compounds from higher plants with lactate dehydrogenase (LDH) and monoacylglycerol lipase (MAGL) inhibitory activities, three new *neo*-clerodane diterpene 12-deacetylsplendidin C (**1**), pseudorosmaricin (**2**), and 2-dehydroxysalvileucanthsin A (**3**) along with six known compounds were isolated from *Salvia pseudorosmarinus* aerial part extracts. Their structures were determined by spectroscopic and spectrometric techniques including 1D- and 2D NMR, and MS analyses. The isolated diterpenes were assayed for their inhibitory activity on LDH5 and MAGL, two enzymes covering key roles in the peculiar energetic metabolism of malignant tumours. All the assayed diterpenes showed negligible activity on LDH5, whereas the known jewenol A (**4**) displayed a moderate inhibition activity on MAGL, showing an $IC_{50}$ value of 46.8 μM and it proved to be a reversible MAGL inhibitor. Docking and molecular dynamic simulation studies where thus performed to evaluate the binding mode of **4** within MAGL.

*Keywords: Salvia pseudorosmarinus*; Lamiaceae; Clerodane diterpenes; Cancer; Monoacylglycerol lipase; Lactate dehydrogenase

## 1. Introduction

It is widely known that most aggressive tumours are characterized by a dysregulated energetic metabolism which affects both glucose and lipid metabolism. Tumour cells are characterized by an addiction to glucose and a marked preferential use of the glycolytic pathway to produce energy even in the presence of abundant oxygen, despite the lower efficiency of glycolysis in the production of ATP from glucose compared to the oxidative phosphorylation. This metabolic shift (Warburg effect) results in an increased rate of glycolysis to compensate the moderate energetic production: the high glucose uptake and the augmented lactate production furnish an adequate energetic refueling to rapidly growing tumour cells [1]. An aberrant lipid metabolism is frequently observed in cancer cells, and many evidences highlight the important role played by lipid metabolism in the development of cancer. The *de novo* fatty acid synthesis is significantly increased in cancer to the detriment of the use of exogenous dietary fatty acids, since the huge amount of internalized glucose is also utilized to synthesize fatty acids by providing building blocks, such as acetyl-CoA. Many of the produced fatty acids are immediately used or they are stored in the cells and they are used on demand, thanks to the enzymatic activity of lipases. Lipids are necessary for the synthesis of membranes of growing tumour cells and for the production of oncogenic signaling molecules [2].

In this context, many proteins are upregulated in tumours, such as enzymes, receptors and effectors of the involved deregulated metabolic pathways. For example, the last enzyme of the glycolytic cascade, the isoform 5 of lactate dehydrogenase (LDH5) plays a pivotal role in the maintenance and progression of tumours. LDH5 is a homotetrameric enzyme composed of four A subunits and it is localized in the cytoplasm. LDH5 catalyzes the conversion of pyruvate, the end product of glycolysis, to lactate, with the concomitant oxidation of the cofactor NADH to $NAD^+$. In this way, lactate is excreted out of the cells, and the acidic extracellular environment facilitates the spread of metastasis, and the regenerated $NAD^+$ allows the glycolytic pathway to continue to

produce energy for tumour cells [3]. In the lipid metabolism, the serine hydrolase monacylglycerol lipase (MAGL) is the enzyme responsible for the hydrolysis of monoacyglycerols to free fatty acids and glycerol in peripheral tissues and it is also the enzyme designated to the catabolism of the endocannabinoid 2-arachidonylglcyerol in the central nervous system. The increased release of stored fatty acids in tumours generated by the intensified MAGL activity is necessary to support cancer growth and the synthesis of lipid messengers, triggering cell migration and aggressiveness [4].

The metabolic reprogramming occurring in most tumours is a therapeutic opportunity: both LDH5 and MAGL represent two attractive anti-cancer targets, since it was demonstrated that their inhibition led to antiproliferative effects *in vitro* and/or *in vivo* [5,6]. Moreover, the inhibition of LDH5 or MAGL can be considered a harmless therapeutic strategy since healthy cells are unaffected, because they do not completely rely on the dysregulated energetic metabolic pathways for their survival. In the last decades, many synthetic and natural compounds showing inhibitory activities on LDH5 [7,8] or MAGL [9,10] were discovered, and there is a great interest for the discovery of new inhibitors of these two enzymes, highlighting that cancer metabolism is an attractive area of investigation. In addition, the interest in the identification of novel MAGL inhibitors is also due to their potential use in the treatment of other pathologies such as chronic and neuropathic pain [11].

The genus *Salvia* (Lamiaceae) consist of over 900 species widely distributed in different regions around the world such as the Mediterranean area, Central Asia, Africa, and America. Some members of this genus have economic importance for their use as flavoring agents in perfumery and cosmetics but are also interesting for their biologically active constituents, particularly diterpenes and phenolics, many of which showed antitumor properties [12]. Moreover, diterpenoids and phenolic derivatives isolated from different *Salvia* species showed antioxidant, anticoagulant, antihypertensive, anti-fibrotic, anti-ischemia-reperfusion injury, and antiviral activities [13]. Although the interest in the genus has increased, only a relatively small number of the known

species have been chemically and biologically explored. In the course of our ongoing research program on compounds from higher plants with LDH5 and MAGL inhibitory activity, *Salvia pseudorosmarinus* Epling was selected as the subject of this investigation. The plant is a perennial shrub up to 150 cm high with purple flowers growing in Peruvian Ande at 3500-4000 m above sea level, where the leaves are used in folk traditional medicine against stomach ache and diarrhea [14]. To the best of our knowledge, this species has been never investigated. In this paper, we describe the isolation and structural characterization of three new *neo*-clerodanes (**1-3**) (Fig. 1), together with six known compounds from *S. pseudorosmarinus* aerial parts, and LDH5 and MAGL inhibitory activity of the isolated diterpenes.

## 2. Experimental

### *2.1. General experimental procedures*

Optical rotations were measured on an Atago AP-300 digital polarimeter equipped with a sodium lamp (589 nm) and a 1 dm microcell. NMR experiments were performed on a Bruker DRX-600 spectrometer (Bruker BioSpin GmBH, Rheinstetten, Germany) equipped with a Bruker 5 mm TCI CryoProbe at 300 K. All 2D NMR spectra were acquired in methanol-$d_4$ (99.95%, Sigma-Aldrich), and standard pulse sequences and phase cycling were used for DQF-COSY, HSQC, and HMBC spectra. ESI-MS were obtained using a Finnigan LC-Q Advantage Termoquest spectrometer, equipped with Xcalibur software. HRESIMS were acquired in the positive ion mode on a LTQ Orbitrap XL mass spectrometer (Thermo Fisher Scientific). TLC were performed on precoated Kieselgel 60 $F_{254}$ plates (Merck); compounds were detected by spraying with $Ce(SO_4)_2/H_2SO_4$ solution. Column chromatographies (CC) were performed over Sephadex LH-20 (40–70 μm, Amersham Pharmacia Biotech AB, Uppsala, Sweden) and Isolera® Biotage® purification system (flash Silica gel 60 SNAP 340 g cartridge, flow rate 100 mL/min); reversed-phase (RP) HPLC

separations were conducted on a Shimadzu LC-20AT series pumping system equipped with a Shimadzu RID10A refractive index detector and a Shimadzu injector, using a $C_{18}$μ-Bondapak column (30 cm x 7.8 mm, 10 μm, Waters-Milford) and a mobile phase consisting of MeOH-$H_2O$ mixtures at a flow rate of 2 mL/min.

*2.2. Plant material*

Aerial parts of *S. pseudorosmarinus* were collected near Cotaparaco, Ancash Province, Peru, in November 2016. The plant was identified by Hamilton Beltram of the Universidad Nacional Mayor de San Marcos, Lima, Peru where a voucher specimen (142-USM-2016) was deposited.

*2.3. Extraction and isolation*

The dried aerial parts of *S. pseudorosmarinus* (1 Kg) were exhaustively extracted with solvents of increasing polarity: *n*-hexane, $CHCl_3$, $CHCl_3$-MeOH (9:1), and MeOH to give 12.8, 41.3, 12.2, and 65.9 g of the respective residues. Part of the $CHCl_3$ residue (5.0 g) was subjected to Isolera Biotage column chromatography (340 g silica SNAP cartridge, flow rate 100 mL/min), eluting with $CHCl_3$ followed by increasing concentrations of MeOH in $CHCl_3$ (between 1% and 100%). Fractions of 27 mL were collected, analysed by TLC and grouped into six major fractions (A-F). Fraction C contained oleanolic acid. Fractions B (872 mg) and D (500 mg) were subjected to RP-HPLC with MeOH-$H_2O$ (4.5:5.5) to give compound **2** (2.0 mg, $t_R$ = 9 min) from fraction B; compound **3** (1.3 mg, $t_R$ = 17 min), from fraction D. Fraction F (646 mg) was purified by RP-HPLC with MeOH-$H_2O$ (1:1) to give compounds **1** (3.1 mg, $t_R$ = 12 min) and **4** (10 mg, $t_R$ = 15 min). Part of the $CHCl_3$-MeOH residue (10.0 g) was submitted to Sephadex LH-20 column chromatography (5 x 75 cm, flow rate 1.5 mL/min) using MeOH as eluent and collecting five major fractions (A-E) grouped by TLC. Fraction C (137 mg) was chromatographed over RP-HPLC with MeOH-$H_2O$ (3.5:6.5) to give

protocatechualdehyde (1.5 mg, $t_R$ = 8 min) and caffeic acid methyl ester (1.6 mg, $t_R$ = 12 min). Fraction E (140 mg) was subjected to RP-HPLC with MeOH-$H_2O$ (1:1) to yield eriodictyol (1.7 mg, $t_R$ = 10 min) and pedalitin (2.5 mg, $t_R$ = 16 min). All the compounds met the criteria of ≥ 94% purity, as inferred by HPLC and NMR analyses.

*2.3.1. 12-deacetylsplendidin C (**1**)*

Pale yellow amorphous powder; $[\alpha]_D^{25}$ -16.3 (*c* 0.1, MeOH); $^1$H ($CD_3OD$, 600 MHz) and $^{13}$C NMR ($CD_3OD$, 150 MHz) data, see Table 1; ESI-MS *m/z* 529 $[M + Na]^+$, 369 $[M + Na - 160]^+$; HR-ESIMS *m/z* 529.2045 $[M + Na]^+$ (calcd for $C_{26}H_{34}O_{10}Na$ 529.2050).

*2.3.2. Pseudorosmaricin (**2**)*

Pale yellow amorphous powder; $[\alpha]_D^{25}$ +44.6 (*c* 0.1, MeOH); $^1$H ($CD_3OD$, 600 MHz) and $^{13}$C NMR ($CD_3OD$, 150 MHz) data, see Table 1; ESI-MS *m/z* 423 $[M - H]^-$, 259 $[M – H - 164]^-$; HR-ESIMS *m/z* 425.2164 $[M + H]^+$ (calcd for $C_{22}H_{33}O_8$ 425.2175).

*2.3.3. 2-Dehydroxysalvileucanthsin A (**3**)*

Pale yellow amorphous powder; $[\alpha]_D^{25}$ +16.2 (*c* 0.1, MeOH); $^1$H ($CD_3OD$, 600 MHz) and $^{13}$C NMR ($CD_3OD$, 150 MHz) data, see Table 1; HR-ESIMS *m/z* 357.1339 $[M + H]^+$ (calcd for $C_{20}H_{21}O_6$ 357.1338).

*2.4. Enzymatic assays*

Compounds **1**-**4** were tested on purified human LDH5 (Lee Biosolution Inc.) and MAGL (Cayman Chemical), as previously reported [15,16]. Compound (4-(4-chlorobenzoyl)piperidin-1-yl)(4-methoxyphenyl)-methanone, named CL6a, is the reference MAGL inhibitor previously synthesized

in our laboratory (purity percentage 99% by HPLC analysis). DMSO stock solutions of the compounds (the concentration of DMSO did not exceed 4% during the measurements) were diluted to obtain seven different concentrations (from 400 to 0.064 μM, in duplicate for each concentration), that were dispensed in 96-well plates to generate the concentration-response curves. Maximum and minimum controls were present in each plate. Both the assays were run at room temperature, at a final volume of 200 μL in each well. The obtained $IC_{50}$ values are the mean of three independent experiments. In LDH assays, the reaction was performed in the "forward" direction (from pyruvate to lactate), in 100 mM phosphate buffer (pH = 7.4) in the presence of 200 μM pyruvate and 40 μM NADH, and the amount of consumed NADH was measured (340 nm) after 15 min incubation. In MAGL assays, the substrate 4-nitrophenylacetate (4-NPA, 100 μM) was converted to 4-nitrophenol, in 10 mM Tris buffer (pH = 7.2) containing 1 mM EDTA and 0.1 mg/mL BSA, and the amount of produced 4-nitrophenol was monitored (405 nm) after 30 min incubation. The final measurement for both assays were performed by using a Victor X3 microplate reader (PerkinElmer) and $IC_{50}$ values were derived from experimental data using the sigmoidal dose-response fitting of GraphPad Prism software.

### *2.5. Molecular modeling*

#### *2.5.1. Molecular docking studies*

Compounds **1**-**4** were built using Maestro [17] and subjected to minimization with Macromodel [18], employing the generalized Born/surface area model to simulate a water environment. The conjugate gradient algorithm, the MMFFs force field and a distance-dependent dielectric constant of 1.0 were used for the minimization, performed until a convergence value of 0.05 kcal/(Å•mol) was reached. The compounds were docked into the X-ray structure of human MAGL in complex with inhibitor ZYH (PDB code 3PE6) [19] using AUTODOCK4.2 [20]. AUTODOCK TOOLS [21]

were used to define the torsion angles in the ligands, to add the solvent model and to assign partial atomic charges (Kollman for the protein and Gasteiger for the ligand). A grid box of 82, 40, and 30 points in the x, y, and z directions, respectively, centered on the co-crystallized ZYH inhibitor was used to define the docking site for AUTODOCK calculations. The energetic maps required for docking were generated with a grid spacing of 0.375 Å and a distance-dependent function of the dielectric constant. Compounds **1-4** were docked using 200 Lamarckian genetic algorithm runs of the AUTODOCK search. During each docking run, 10'000'000 steps of energy evaluation were performed and a maximum of 10'000'000 generations were simulated starting from an initial population of 500 individuals. The final docking solutions were clustered together using an rms cut-off of 2.0 Å and leaving all other settings as their defaults. The clusters of solutions with a population higher than 5%, i.e. including more than 5% of all the generated docking poses, were taken into account.

*2.5.2. Molecular dynamic simulations*

Molecular Dynamic simulations were carried out using AMBER 14 [22]. The four MAGL-**4** and the three MAGL-**1** complexes were solvated with a 15 Å water cap within a parallelepiped box; sodium ions were then added as counterions for neutralizing the system. General amber force field (GAFF) parameters were assigned to the ligands, while partial charges were calculated using the AM1-BCC method. Initially, the complexes were subjected to energy minimization through 5'000 steps of steepest descent followed by conjugate gradient, until a convergence of 0.05 kcal/(mol·Å$^2$) was reached. The minimized systems were used as starting point for an MD simulations protocol composed of three steps. In the first one, 0.5 ns of constant-volume simulation were performed, raising the temperature of the system from 0 to 300 K. In the second step, the system was equilibrated through a 3 ns constant-pressure simulation where the temperature was kept constant at 300 K by using the Langevin thermostat. In both the minimization and the first two MD steps, a

harmonic potential of 10 kcal/(mol·Å$^2$) was applied to the protein α carbons. In the third and last MD step, 26.5 ns of constant-pressure simulation were performed without any position restraint, thus leaving the whole system free. A total of 30 ns of simulation was thus performed for each complex. All MD steps were run using particle mesh Ewald electrostatics and periodic boundary conditions [23], a cutoff of 10 Å for the non-bonded interactions and SHAKE algorithm to keep rigid all bonds involving hydrogen.

*2.5.3. Binding energy evaluation*

Relative binding free energy evaluations were performed using AMBER 14. The trajectories extracted from the last 20 ns of each simulation were used for the calculation, for a total of 200 snapshots (at time intervals of 100 ps). Van der Waals, electrostatic and internal interactions were calculated with the SANDER module of AMBER 14, whereas the Generalized Born and the Poisson−Boltzman methods were employed to estimate polar energies through the MM-PBSA module of AMBER 14. Gas and water phases were represented using dielectric constants of 1 and 80, respectively, while nonpolar energies were calculated with MOLSURF program. The entropic term was considered as approximately constant in the comparison of the ligand−protein energetic interactions.

## 3. Results and discussion

The molecular formula of compound **1** ($C_{26}H_{34}O_{10}$) was established by $^{13}C$ NMR and HR-MS (obsd *m/z* 529.2045 for $[M + Na]^+$, calcd *m/z* 529.2050). The ESI MS spectrum of **1** showed a sodiated ion peak at *m/z* 529 $[M + Na]^+$ and a fragment at *m/z* 369 $[M + Na - 160]^+$, due to the loss of a keto hexose moiety. Analysis of $^1H$ and $^{13}C$ NMR data (Table 1) suggested the presence of a

diterpenoid aglycone and a sugar moiety. The $^{1}$H NMR data revealed two methyl groups, of which one singlet (δ 0.82) and one doublet (δ 1.23), a furan ring (δ 6.52, 7.51, 7.52), a trisubstituted double bond, two hydroxymethines at δ 4.28 and 4.73, one hydroxymethylene at δ 3.95 and 5.52, together with the characteristic resonances of a keto sugar, evidenced by signals at $\delta_H$ 4.14 and 4.25 [24]. The $^{13}$C NMR spectrum of **1** was in complete agreement with the previously reported data of other clerodane diterpenes isolated from the genus *Salvia* containing the same open C-ring [25,26]. The elucidation of the whole skeleton in **1** was achieved on the basis of 1D TOCSY, COSY, HSQC, and HMBC correlations, which also allowed the assignment of all the resonances in the $^{13}$C NMR spectrum. The two hydroxymethines were placed at C-7 and C-12, from the HMBC correlations between H-6—C-7, Me-17—C-7 and H-12—C-9, H-12—C-11, H-12—C-14. The structure of the sugar moiety was suggested as D-ribohexo-3-ulopyranoside (3-keto-glucopyranoside) from the chemical shifts of H-1' to $H_2$-6' in the $^{1}$H NMR spectrum and their HSQC correlations with the respective carbons [27,28]. Elucidation of the relative stereochemistry of **1** was mostly based on the close similarities of its NMR data and coupling constant to those of the similar compound splendidin C, isolated from *Salvia splendens* Sellow ex Schult. [29] and from which **1** differed only for the absence of the acetyl group at C-12. Thus, **1** was assigned as 12-deacetylsplendidin C.

In the ESI-MS spectrum of **2** a molecular ion at *m/z* 423 $[M - H]^-$ and a prominent fragment due to the loss of 164 uma (*m/z* 259) were observed. Thus, the molecular formula of **2** was $C_{22}H_{32}O_8$, which required a rearranged diterpenoid skeleton (HR-MS *m/z* 425.2164 $[M + H]^+$, calcd for 425.2175). The 22 carbon signals in the $^{13}$C NMR spectrum (Table 1) were established as one carboxyl moiety, two $sp^2$ carbons, six methylenes (one oxygenated), five methines (four oxygenated), two methyls, two methoxy groups, and four quaternary carbons. In the $^{1}$H NMR spectrum (Table 1) two methyl singlets at δ 0.87 and 1.22 were observed, together with a hydroxymethylene at δ 4.03 and 4.46 and a hydroxymethine at δ 4.31, correlating in the HSQC spectrum with the signals at 71.3 and 77.1 ppm, respectively. Four spin systems were recognized from 1D TOCSY and COSY spectra: H-10—H-2, H-6—H-7, H-11—H-12, H-14—H-15, while the

hydroxymethine signal was established to be involved in an ether bridge between the C-8 and C-12 carbons, on the basis of HMBC experiment, as found in dehydrokerlin, a clerodane diterpene isolated from *Salvia rhyacophila* (Fernald) Epling [30]. The most striking features of the $^{1}$H NMR spectrum of **2**, as compared to dehydrokerlin, were the absence of furanoid protons and the presence of two additional methoxyl signals (δ 3.38, 3.46) and three oxymethine protons (δ 3.86, 4.80, 4.90). Key correlations in the HMBC experiment were observed between H-12—C-13, H-14—C-12, H-14—C-15, H-16—C-14, H-16—C-15 and the two methoxyl groups and C-15 and C-16 respectively, leading to construct a quite rare 2,5-dimethoxy-3,4-dihydroxy-tetrahydrofuran system as E ring. To the best of our knowledge, this side chain has been only found in some clerodane diterpenes isolated from *Salvia divinorum* Epling & Játiva [31] and *Dichrocephala benthamii* C.B. Clarke [32] and in some limonoids from Meliaceae family [33,34]. Other remaining $^{1}$H and $^{13}$C NMR signals were assigned with the aid of 2D NMR spectra. The relative configuration of **2** was established by NOESY correlations and analysis of coupling constant. NOE cross peaks between Me-17—Me-20, $H_2$-19—Me-20, H-10—H-12 established the relative position of the methyl groups and of H-10 as in dehydrokerlin [30], while correlations between H-12—H-14, H-14—H-15, H-16—OMe at C-15, could suggest that these H-atoms were on the same face of the tetrahydrofuran ring. Thus, the structure of **2** was proposed as depicted in Fig. 1, and named pseudorosmaricin.

Compound **3** ($C_{20}H_{20}O_6$) showed a protonated ion peak at *m/z* 357.1339 $[M + H]^+$ (calcd for 357.1338) in the positive HR-MS. The $^{1}$H NMR spectrum (Table 1) revealed the presence of a typical β-monosubstitued furan ring (δ 6.55, 7.58, 7.62), one methyl (δ 0.90), one double bond (δ 6.84), two hydroxymethines (δ 5.13, 5.70), two methines (δ 1.68, 2.77), one hydroxymethylene (δ 4.13), and two methylenes (δ 1.43, 1.91, 2.28, 2.48). The $^{13}$C NMR data (Table 1) were in agreement with a *neo*-clerodane skeleton for compound **3** as the one reported for blepharolide A, isolated from *Salvia blepharophylla* Brandegee ex Epling [35] and salvileucanthsin A isolated from *Salvia leucantha* Cav. [36]. Again with the help of 1D TOCSY, COSY, HSQC, and HMBC experiments the total structure of **3** was deduced; particularly according to HMBC spectrum the

hydroxymethylene protons at δ 4.13 ($H_2$-19) showed a long range correlation with C-6 and C-18, the double bond proton at δ 6.84 (H-3) with C-5, the methine at δ 2.77 (H-11) with C-7, C-9, C-10, C-12, and C-17, the hydroxymethine at δ 5.70 (H-12) with C-8, C-13, and C-16, the hydroxymethine at δ 5.13 (H-7) with C-9, C-11, and C-17, the methylene protons at δ 2.28 and 2.48 ($H_2$-2) with C-3, C-5, and C-10. The relative stereochemistry of **3** was assigned by coupling constant analysis and comparison with those of similar compound salvileucanthsin A [36], from which **3** differed only for the absence of the hydroxy group at C-2. Thus, new compound **3** was characterized as 2-dehydroxysalvileucanthsin A.

On the basis of NMR and MS data and in comparison with the literature, the chemical structures of six known compounds were identified as jewenol A (**4**) [37], eriodictyol [38], pedalitin [39], protocatechualdehyde [40], oleanolic acid [41], and caffeic acid methyl ester [42].

The isolated diterpenes **1**-**4** were tested on purified human LDH5 and MAGL enzymes to determine if they showed a certain inhibition potency, in the presence of two reference compounds, the LDH5 inhibitor galloflavin [43] or the MAGL inhibitor CL6a [9]. All the tested compounds were inactive on LDH5, showing $IC_{50}$ values greater than 200 μM (Table 2). In the MAGL enzymatic assay, none compound showed any inhibition activity, with the exception of **4** that displayed a notable $IC_{50}$ value in the low micromolar range (46.8 μM, Table 2). This promising result led us to further investigate the binding mechanism of this MAGL inhibitor. First of all, we verified if jewenol A could interact with cysteine residues of the protein: compound **4** was tested in the presence of the thiol derivative 1,4-dithio-DL-threitol (DTT). As shown in Fig. 2A, the activity of compound **4** remained almost unaltered in the presence of 100 μM DTT, since the initial $IC_{50}$ value of 46.8 μM was only minimally increased to 50.1 μM, thus demonstrating that the inhibition potency of jewenol A was not affected by the presence of a cysteine-mimicking compound, therefore excluding any possible interaction with cysteines of MAGL. Moreover, the effect of preincubation time on the inhibitory activity of compound **4** was determined in order to establish whether the inhibition mechanism was reversible or irreversible. We evaluated the inhibitory

potency of **4** at different preincubation times of the compound with the enzyme: compound **4** was preincubated for 0, 30 or 60 min with the enzyme before the addition of the substrate to start the enzymatic reaction. If the inhibitor irreversibly inhibits the enzyme, an increased inhibitory activity should result at longer incubation times, differently if the compound behaves as a reversible inhibitor, the inhibition potency should be constant, being independent of the incubation time. Fig. 2B showed the $IC_{50}$ values of **4** at different incubation times and it is evident that the inhibitory potency did not show a significant increase at longer incubation times, confirming that jewenol A was a reversible MAGL inhibitor.

In order to evaluate how **4** can interact with MAGL, docking and molecular dynamics (MD) simulation studies followed by ligand-protein binding energy evaluations were carried out. Jewenol A was docked into the X-ray structure of human MAGL in complex with inhibitor ZYH (PDB code 3PE6) [19] using a thorough AUTODOCK [20] procedure that produced good results in both virtual screening and pose prediction studies [44,45]. The docking protocol generated 200 different docking solutions, which were then clustered based on their reciprocal root-mean square (RMSD) deviation using a cut-off of 2.0 Å. Four different clusters of binding poses where then obtained and, for each of them, the docking solution associated with the best estimated binding energy was selected as a representative binding mode. The reliability of all binding modes was thus evaluated by subjecting the four MAGL-**4** complexes to MD simulation studies. A simulation protocol consisting of a total of 30 ns of MD simulation, which was already successfully used for pose prediction analyses of natural compounds [45], was applied on the four complexes. The results were then analyzed in terms of RMSD of protein α carbons and ligand disposition during the simulation with respect to their coordinates in the starting complex. In all simulations, the protein demonstrated a remarkable stability, since after only 5-10 ns the α carbons RMSDs reached an equilibrium, showing a roughly constant value around 1.2 Å (Fig. 3), thus confirming the reliability of the MD protocol employed. The analysis of the ligand trajectory during the simulation highlighted a particular stability for pose 2, since it showed an average RMSD of 1.3 Å, whereas in the other

three poses the RMSD of the ligand ranged from 2.4 to 2.7 Å. In order to further confirm the reliability of the MD protocol, the same protocol was also applied on the reference MAGL-ZYH X-ray complex. As expected, the analysis of the RMSD of the protein α carbons showed results similar to those obtained for the MAGL-**4** complexes and the reference ligand ZYH perfectly maintained the experimental binding mode, as the average RMSD of its disposition during the simulation corresponded to 0.9 Å (Figure S16, Supporting Information).

The four MAGL-**4** complexes were then subjected to binding energy evaluation [46, 47], which were performed applying the Molecular Mechanic-Generalized Born surface area (MM-GBSA) and the Molecular Mechanic-Poisson Boltzmann surface area (MM-PBSA) methods [48] on the MD trajectories relative to the last 20 ns of simulation. The analysis confirmed pose 2 as the most reliable binding mode, being associated to the best ligand-protein binding affinity according to both evaluation methods (ΔGBSA = -55.0 kcal/mol; ΔPBSA = -29.6 kcal/mol) and exceeding of about 5-8 kcal/mol, at least, the interaction energies estimated for the other poses using the MM-PBSA and MM-GBSA methods, respectively (Table S1, Supporting Information). Fig. 4 showed the minimized average structure of MAGL in complex with jewenol A in the predicted binding mode 2 obtained from the last 20 ns of MD simulation. The ligand is located in the acyl-chain binding region, the big hydrophobic portion of the enzyme catalytic site that welcomes the fatty acid chain of its natural substrate 2-AG. This region, where also other noncovalent ligands are supposed to bind [49], is the same occupied by the cyclohexylbenzoxazole moiety of the reference inhibitor ZYH in the corresponding X-ray structure (Figure S17, Supporting Information) [19]. In particular, the bicyclic core of compound **4** is placed in the lipophilic pocket constituted by A151, A156, F159, L205, G210, L213 and L214, thus forming hydrophobic interactions with all these residues, while the lateral chain of the molecule takes contact with L148, I179 and L241. The two hydroxymethyl substituents connected to the ligand core do not seem to establish important interactions with the protein. On the contrary, the terminal hydroxyl group on the ligand lateral chain is placed in a particular subpocket of the binding site called oxyanion hole, which is essential to stabilize the

transition state of the catalytic reaction [19]. Through this OH group, the ligand forms H-bonds with the backbone nitrogen of A51 and with the side chain of S122, which is a key residue for the catalytic activity of the enzyme, and also forms an intramolecular H-bond with the other hydroxyl group of the chain. Interestingly, the terminal OH group of compound **4** partially mimics the carbonyl moiety of the reference inhibitor ZYH, which is placed in the same subpocket and forms an analogous H-bond with A51 as well as an additional H-bond with M123 (Figure S17).

With the aim of further validating the reliability of the computational approach used to predict the binding mode of compound **4**, the three diterpenes **1**-**3** that proved to be inactive against human MAGL were studied as a control. The compounds were thus docked into the X-ray structure of human MAGL, obtaining three different clusters of poses for compound **1**, two clusters for compound **2** and a single cluster for **3**. The results produced for compounds **2** and **3** suggested that the molecules can not properly bind to MAGL. In fact, in all the generated binding modes, these compounds were predominantly placed outside the binding site of the protein, without reaching the oxyanion hole. Therefore, they could not form any of the H-bonds with A51, M123 and the catalytic S122 showed by the reference inhibitor ZYH or predicted for compound **4**. For this reason, the docking results obtained for compounds **2** and **3** were already sufficient to discard the two diterpenes as potential MAGL inhibitors. Compound **1** was predicted to interact with the oxyanion hole in one out of the three binding poses generated by docking. For this reason, the three binding modes calculated for compound **1** were further studied through MD simulations and binding energy evaluations. However, contrarily to the results obtained for compound **4**, the protocol did not highlight any of the three binding poses as more reliable than the other ones. In fact, none of the three binding modes showed a particular stability with respect to the others in terms of RMSD of the ligand disposition during the MD and none of them was associated to a ligand-protein binding affinity higher than those calculated for the other poses according to both the evaluation methods used (Figure S18, Supporting Information). Moreover, the calculated binding affinity values resulted to be at least 11-15 kcal/mol lower than those associated to the binding mode predicted for

the active compound **4**. These results suggest that compound **1** is not an inhibitor of human MAGL. Overall, the results obtained by applying the docking, MD and binding energy evaluation protocol on compounds **1-3** are in agreement with the inactivity of the compounds towards MAGL, and thus further validate the reliability of the computational procedures herein applied and the binding mode predicted for the active compound **4**.

## 4. Conclusion

In summary, three new *neo*-clerodane diterpenes and six known compounds were isolated from *Salvia pseudorosmarinus* aerial parts. The known diterpene jewenol A (**4**) exhibited a moderate inhibition activity on MAGL, as a reversible inhibitor. Previously, another natural diterpene, tanshinone IIA, obtained from *Salvia divinorum* Epling & Játiva, was found to inhibit MAGL [50]. Docking and molecular dynamic simulation studies suggested that **4** could bind to the acyl-chain binding region of the enzyme. To our knowledge, this is the first report of naturally occurring *neo*-clerodane as MAGL inhibitor and could suggest its skeleton as a starting chemical scaffold for future investigation on plant small molecules as potential MAGL inhibitors.

## Conflict of interest

The authors declare that there is no conflict of interest.

## Supplementary data

Supplementary data to this article can be found on line, at….

**References**


[1] R.B. Hamanaka, N.S. Chandel, Targeting glucose metabolism for cancer therapy, J. Exp. Med. 209 (2012) 211-215.

[2] C.R. Santos, A. Schulze, Lipid metabolism in cancer, FEBS J. 279 (201) 2610-2623.

[3] C. Granchi, S. Bertini, M. Macchia, F. Minutolo, Inhibitors of lactate dehydrogenase isoforms and their therapeutic potentials, Curr. Med. Chem. 17 (2010) 672-697.

[4] D.K. Nomura, J.Z. Long, S. Niessen, H.S. Hoover, S.W.Ng, B.F. Cravatt, Monoacylglycerol lipase regulates a fatty acid network that promotes cancer pathogenesis, Cell 140 (2010) 49-61.

[5] V.R. Fantin, J. St-Pierre, P. Leder, Attenuation of LDH-A expression uncovers a link between glycolysis, mitochondrial physiology, and tumor maintenance, Cancer Cell 9 (2006) 425-434.

[6] M. Ma, J. Bai, Y. Ling, W. Chang, G. Xie, R. Li, G. Wang, K. Tao, Monoacylglycerol lipase inhibitor JZL184 regulates apoptosis and migration of colorectal cancer cells, Mol. Med. Rep. 13 (2016) 2850-2856.

[7] C. Granchi, S. Roy, C. Del Fiandra, T. Tuccinardi, M. Lanza, L. Betti, G. Giannaccini, A. Lucacchini, A. Martinelli, M. Macchia, F. Minutolo, Triazole-substituted *N*-hydroxyindol-2-carboxylates as inhibitors of isoform 5 of human lactate dehydrogenase (hLDH5), Medchemcomm. 2 (2011) 638-643.

[8] G. Rai, K.R. Brimacombe, B.T. Mott, D.J. Urban, X. Hu, S.M. Yang, T.D. Lee, D.M. Cheff, J. Kouznetsova, G.A. Benavides, K. Pohida, E.J. Kuenstner, D.K. Luci, C.M. Lukacs, D.R. Davies, D.M. Dranow, H. Zhu, G. Sulikowski, W.J. Moore, G.M. Stott, A.J. Flint, M.D. Hall, V.M. Darley-Usmar, L.M. Neckers, C.V. Dang, A.G. Waterson, A. Simeonov, A. Jadhav, D.J. Maloney, Discovery and optimization of potent, cell-active pyrazole-based inhibitors of lactate dehydrogenase (LDH), J. Med. Chem. 60 (2017) 9184-9204.

[9] T. Tuccinardi, C. Granchi, F. Rizzolio, I. Caligiuri, V. Battistello, G. Toffoli, F. Minutolo, M. Macchia, A. Martinelli, Identification and characterization of a new reversible MAGL inhibitor, Bioorg. Med. Chem. 22 (2014) 3285-3291.

[10] A. Chicca, J. Marazzi, J. Gertsch, The antinociceptive triterpene β-amyrin inhibits 2-arachidonoylglycerol (2-AG) hydrolysis without directly targeting cannabinoid receptors, Br. J. Pharmacol. 167 (2012) 1596-1608.

[11] L. Monti, A. Stefanucci, S. Pieretti, F. Marzoli, L. Fidanza, A. Mollica, S. Mirzaie, S. Carradori, L. De Petrocellis, A. Schiano Moriello, S. Benyhe, F. Zádor, E. Szűcs, F. Ötvös, A.I. Erdei, R. Samavati, S. Dvorácskó, C. Tömböly, E. Novellino, Evaluation of the analgesic effect of 4-anilidopiperidine scaffold containing ureas and carbamates, J. Enzyme Inhib. Med. Chem. 31 (2016) 1638-1647.

[12] D.C. Hao, G.B. Ge, P.G. Xiao, Anticancer drug targets of *Salvia* phytometabolites: chemistry, biology and omics, Curr. Drug Targets 19 (2018) 1-20.

[13] Y.B. Wu, Z.Y. Ni, Q.W. Shi, M. Dong, H. Kiyota, Y.C. Gu, B. Cong, Constituents from *Salvia* species and their biological activities, Chem. Rev. 112 (2012) 5967-6026.

[14] B. Alvarado, Plantas Medicinales de la Cordillera Negra, Primera Edición, Emprograf, Lima, 2003.

[15] A. Bader, T. Tuccinardi, C. Granchi, A. Martinelli, M. Macchia, F. Minutolo, N. De Tommasi, A. Braca, Phenylpropanoids and flavonoids from *Phlomis kurdica* as inhibitors of human lactate dehydrogenase, Phytochemistry 116 (2015) 262-268.

[16] K.A. Beladjila, D. Berrehal, N. De Tommasi, C. Granchi, G. Bononi, A. Braca, M. De Leo, New phenylethanoid glycosides from *Cistanche phelypaea* and their activity as inhibitors of monoacylglycerol lipase (MAGL), Planta Med. 84 (2018) 710-715.

[17] Maestro, version 9.0; Schrödinger Inc: Portland, OR, 2009.

[18] Macromodel, version 9.7; Schrödinger Inc: Portland, OR, 2009.

[19] C. Schalk-Hihi, C. Schubert, R. Alexander, S. Bayoumy, J.C. Clemente, I. Deckman, R.L. DesJarlais, K.C. Dzordzorme, C.M. Flores, B. Grasberger, J.K. Kranz, F. Lewandowski, L. Liu, H. Ma, D. Maguire, M.J. Macielag, M.E. McDonnell, T. Mezzasalma Haarlander, R. Miller, C. Milligan, C. Reynolds, L.C. Kuo, Crystal structure of a soluble form of human monoglyceride lipase in complex with an inhibitor at 1.35 Å resolution, Protein Sci. 20 (2011) 670-683.

[20] G.M. Morris, R. Huey, W. Lindstrom, M.F. Sanner, R.K. Belew, D.S. Goodsell, A.J. Olson, AutoDock4 and AutoDockTools4: automated docking with selective receptor flexibility, J. Comput. Chem. 30 (2009) 2785-2791.

[21] M.F. Sanner, Python: a programming language for software integration and development, J. Mol. Graphics Modell. 17 (1999) 57-61.

[22] D.A. Case, J.T. Berryman, R.M. Betz, D.S. Cerutti, T.E. III Cheatham, T.A. Darden, R.E. Duke, T.J. Giese, H. Gohlke, A.W. Goetz, N. Homeyer, S. Izadi, P. Janowski, J. Kaus, A. Kovalenko, T.S. Lee, S. LeGrand, P. Li, T. Luchko, R. Luo, B. Madej, K.M. Merz, G. Monard, P. Needham, H. Nguyen, H.T. Nguyen, I. Omelyan, A. Onufriev, D.R. Roe, A. Roitberg, R. Salomon-Ferrer, C.L. Simmerling, W. Smith, J. Swails, R.C. Walker, J. Wang, R.M. Wolf, X. Wu, D.M. York, P.A. Kollman, AMBER 2015, University of California, San Francisco.

[23] D.M. York, T.A. Darden, L.G. Pedersen, The effect of long-range electrostatic interactions in simulations of macromolecular crystals: a comparison of the Ewald and truncated list methods, J. Chem. Phys. 99 (1993) 8345-8348.

[24] B. Gering, P. Junior, M. Wichtl, Iridoid glycoside from *Penstemon confertus*, Phytochemistry 26 (1987) 3011-3013.

[25] G. Fontana, G. Savona, B. Rodriguez, Clerodane diterpenoids from *Salvia splendens*, J. Nat. Prod. 69 (2006) 1734-1738.

[26] A. Bisio, N. De Tommasi, G. Romussi, Diterpenoids from *Salvia wagneriana*, Planta Med. 70 (2004) 452-457.

[27] T. Iwagawa, T. Hase, Iridoid glycosides from *Viburnum suspensum*, Phytochemistry 28 (1989) 2393-2396.

[28] M. Fan, Y. Zhu, Z.J. Zhang, R.N. Du, Q.F. Zhu, X.D. Wu, Q.S. Zhao, Salvihispin A and its glycoside, two *neo*-clerodane diterpenoids with neurotrophic activities from *Salvia hispanica* L., Tetrahedron Lett. 59 (2018) 143-146.

[29] Z.H. Pan, J.T. Cheng, J. He, Y.Y. Wang, L.Y. Peng, G. Xu, W.B. Sun, Q.S. Zhao, Splendidins A-C, three new clerodane diterpenoids from *Salvia splendens*, Helv. Chim. Acta 94 (2011) 417-422.

[30] M.C. Fernández, B. Esquivel, J. Cárdenas, A.A. Sánchez, R.A. Toscano, L. Rodríguez-Hahn, Clerodane and aromatic seco-clerodane diterpenoids from *Salvia rhyacophila*, Tetrahedron 47 (1991) 7199-7208.

[31] W.W. Harding, K. Tidgewell, M. Schmidt, K. Shah, C.M. Dersch, J. Snyder, D. Parrish, J.R. Deschampos, R.B. Rothman, T.E. Prisinzano, Salvinicins A and B, new neoclerodane diterpenes from *Salvia divinorum*, Organic Lett. 7 (2005) 3017-3020.

[32] B. Song, G. Ding, X.H. Tian, L. Li, C. Zhou, Q.B. Zhang, M.H. Wang, T. Zhang, Z.M. Zou, Anti-HIV-1 integrase diterpenoids from *Dichrocephala benthamii*, Phytochemistry Lett. 14 (2015) 249-253.

[33] L.L. Wang, C.S. Jiang, Y. Fu, F.F. Chen, L.F. Lan, H.Y. Zhang, Y.W. Guo, Two new limonoids from the root bark of Chinese medicinal plant *Dictamnus dasycarpus*, Helv. Chim. Acta 97 (2014) 1301-1306.

[34] C. Muñoz Camero, A. Vassallo, M. De Leo, A. Temraz, N. De Tommasi, A. Braca, Limonoids from *Aphanamixis polystachya* leaves and their interaction with Hsp90, Planta Med. 2018 in press (DOI: 10.1055/a-0624-9538).

[35] A. Bisio, N. Fontana, G. Romussi, G. Ciarallo, N. De Tommasi, C. Pizza, A. Mugnoli, Clerodane diterpenoids from *Salvia blepharophylla*, Phytochemistry 52 (1999) 1535-1540.

[36] Y.J. Jiang, J. Su, X. Shi, X.D. Wu, X.Q. Chen, J. He, L.D. Shao, X.N. Li, L.Y. Peng, R.T. Li, Q.S. Zhao, *neo*-Clerodanes from the aerial parts of *Salvia leucantha*, Tetrahedron 72 (2016) 5507-5514.

[37] A. Ohsaki, N. Ohno, K. Shibata, T. Tokoroyama, T. Kubota, K. Hirotsu, T. Higuchi, Minor diterpenoids from *Portulaca* cv. Jewel, Phytochemistry 27 (1988) 2171-2173.

[38] P.K. Agrawal, Carbon-13 NMR of Flavonoids, Elsevier, Amsterdam, 1989, 106.

[39] N. Bai, K. He, Z. Zhou, C.S. Lai, L. Zhang, Z. Quan, X. Shao, M.H. Pan, C.T. Ho, Flavonoids from *Rabdosia rubescens* exert anti-inflammatory and growth inhibitory effect against human leukemia HL-60 cells, Food Chem. 122 (2010) 831-835.

[40] N. Syafni, D.P. Putra, D. Arbain, 3,4-Dihydroxybenzoic acid and 3,4-dihydroxybenzaldehyde from the fern *Trichomanes chinense* L.; isolation, antimicrobial and antioxidant properties, Indonesian J. Chem. 12 (2012) 273-278.

[41] S.B. Mahato, A.P. Kundo, $^{13}$C NMR spectra of pentacyclic triterpenoids-A compilation and some salient features, Phytochemistry 37 (1994) 1517-1575.

[42] M. Saleem, H.J. Kim, C. Jin, Y.S. Lee, Antioxidant caffeic acid derivatives from leaves of *Parthenocissus tricuspidata*, Arch. Pharm. Res. 27 (2004) 300-304.

[43] M. Manerba, M. Vettraino, L. Fiume, G. Di Stefano, A. Sartini, E. Giacomini, R. Buonfiglio, M. Roberti, M. Recanatini, Galloflavin (CAS 568-80-9): a novel inhibitor of lactate dehydrogenase, ChemMedChem 7 (2012) 311-317.

[44] G. Poli, A. Gelain, F. Porta, A. Asai, A. Martinelli, T. Tuccinardi, Identification of a new STAT3 dimerization inhibitor through a pharmacophore-based virtual screening approach, J. Enzyme Inhib. Med. Chem. 31 (2016) 1011-1017.

[45] F. Dal Piaz, M.B. Vera Saltos, S. Franceschelli, G. Forte, S. Marzocco, T. Tuccinardi, G. Poli, S. Nejad Ebrahimi, M. Hamburger, N. De Tommasi, A. Braca, Drug Affinity Responsive Target Stability (DARTS) identifies laurifolioside as a new clathrin heavy chain modulator, J. Nat. Prod. 79 (2016) 2681-2692.

[46] C. Granchi, I. Caligiuri, E. Bertelli, G. Poli, F. Rizzolio, M. Macchia, A. Martinelli, F. Minutolo, T. Tuccinardi, Development of terphenyl-2-methyloxazol-5(4H)-one derivatives as selective reversible MAGL inhibitors, J. Enzyme Inhib. Med. Chem. 32 (2017) 1240-1252.

[47] G. Zengin, I. Senkardes, A. Mollica, C.M.N. Picot-Allain, G. Bulut, A. Dogan, M.F. Mahomoodally, New insights into the in vitro biological effects, in silico docking and chemical profile of clary sage - Salvia sclarea L, Comput. Biol. Chem. 75 (2018) 111-119.

[48] P.A. Kollman, I. Massova, C. Reyes, B. Kuhn, S. Huo, L. Chong, M. Lee, T. Lee, Y. Duan, W. Wang, O. Donini, P. Cieplak, J. Srinivasan, D.A. Case, T.E. Cheatham, Calculating structures and free energies of complex molecules: combining molecular mechanics and continuum models, Acc. Chem. Res. 33 (2000) 889-897.

[49] G. Bononi, C. Granchi, M. Lapillo, M. Giannotti, D. Nieri, S. Fortunato, M.E. Boustani, I. Caligiuri, G. Poli, K.E. Carlson, S.H. Kim, M. Macchia, A. Martinelli, F. Rizzolio, A. Chicca, J.A. Katzenellenbogen, F. Minutolo, T. Tuccinardi. Discovery of long-chain salicylketoxime derivatives as monoacylglycerol lipase (MAGL) inhibitors, Eur. J. Med. Chem. 157 (2018) 817-836.

[50] R. Yang, Y. Lu, J. Liu., Identification of tanshinone IIA as a natural monoacylglycerol lipase inhibitor by combined *in silico* and *in vitro* approach, Med. Chem. Commun. 5 (2014) 1528-1532.

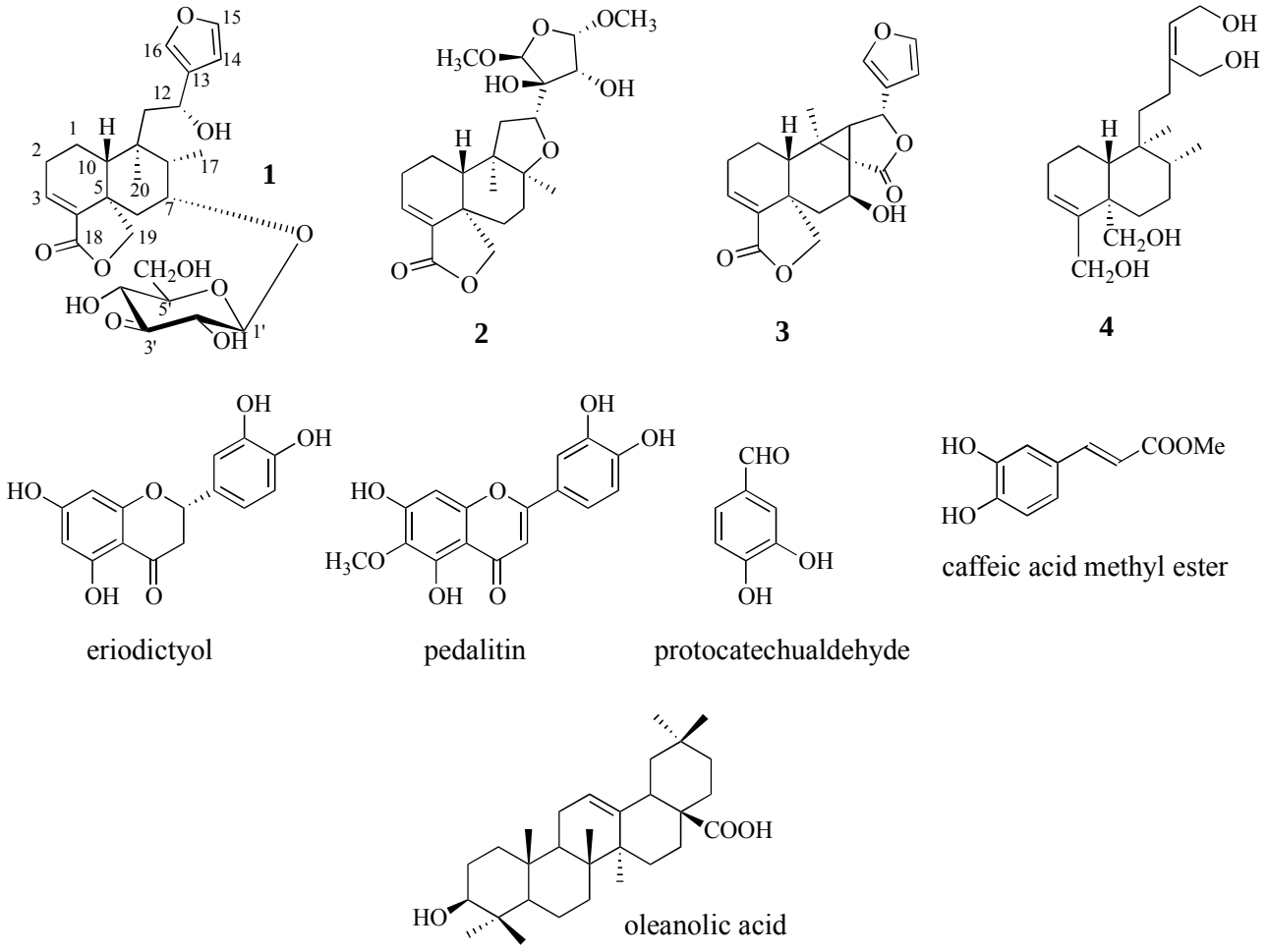


**Fig. 1.** Chemical structures of compounds isolated from *Salvia pseudorosmarinus*.

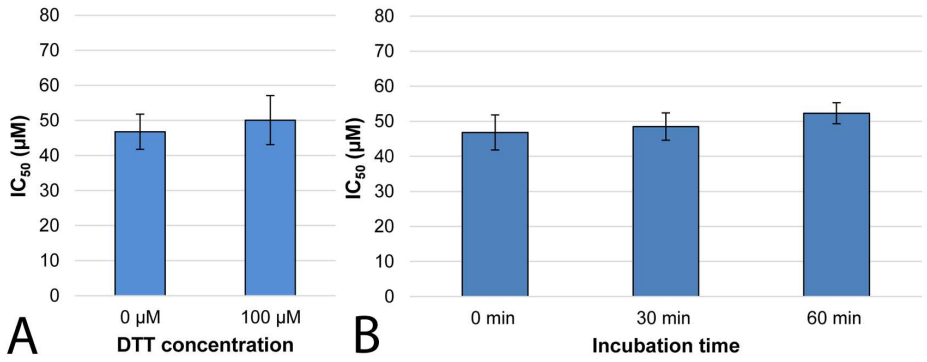


**Fig. 2.** Compound **4**-MAGL inhibition analysis. A) Effect of DTT (0 or 100 μM) on MAGL inhibition. B) Preincubation assay: inhibition values of **4** at different preincubation times with MAGL (0, 30, and 60 min).

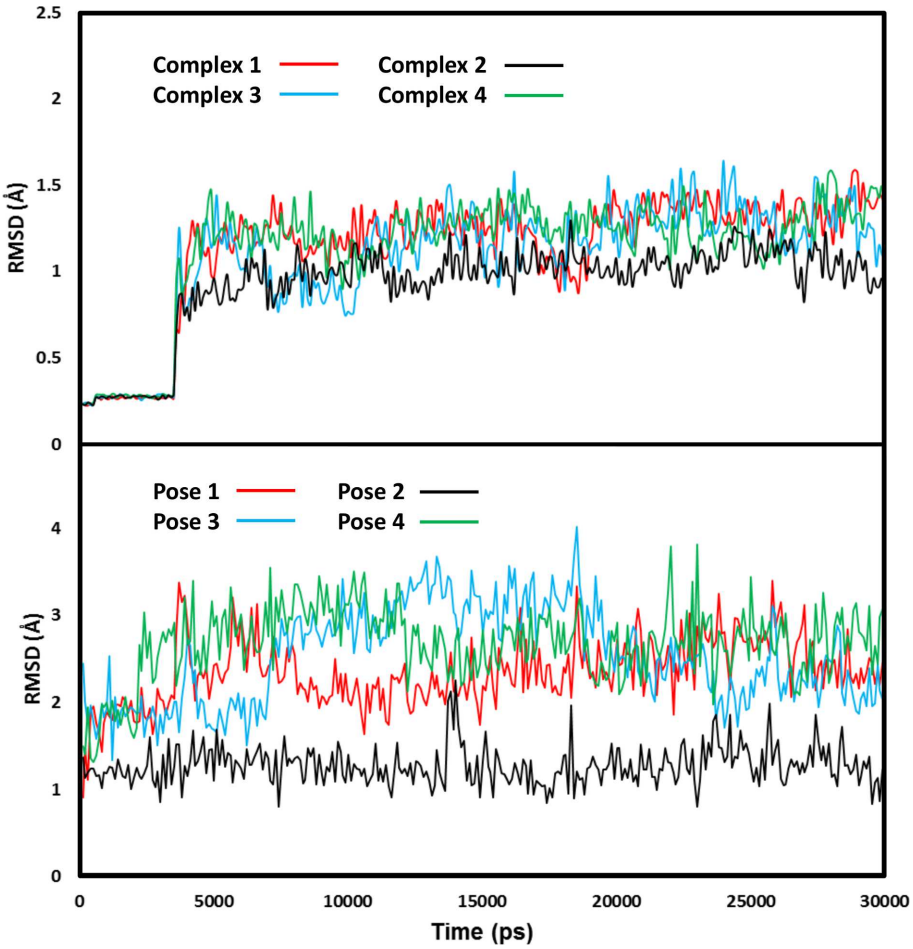


**Fig. 3.** MD analysis of the four MAGL-compound **4** complexes. In the first plot the RMSD of the protein α-carbons during the simulation from their crystallographic coordinates are shown; the second plot reports the RMSD of the ligand disposition with respect to its initial docking pose.

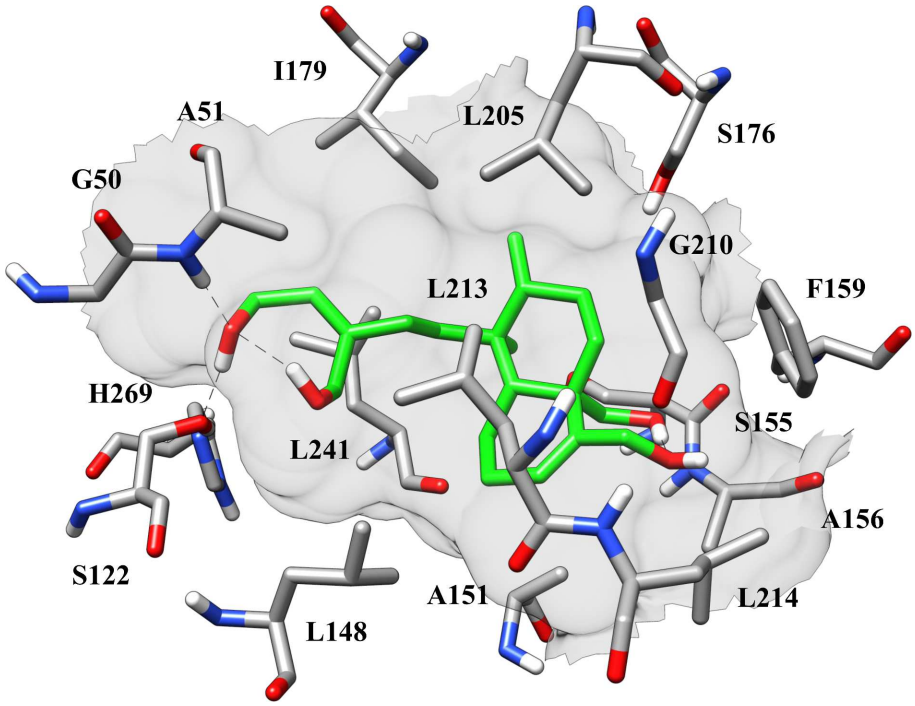


**Fig. 4.** Minimized average structure of **4** within the catalytic site of human MAGL in binding mode 2, derived from the last 20 ns of MD simulation. Hydrogen bonds are represented as black dashed lines.

**Table 1**

$^{1}H$ ($CD_3OD$, 600 MHz) and $^{13}C$-NMR ($CD_3OD$, 150 MHz) data of compounds **1-3**[a].

| | **1** | | **2** | | **3** | |
|---|---|---|---|---|---|---|
| position | $\delta_H$ | $\delta_C$ | $\delta_H$ | $\delta_C$ | $\delta_H$ | $\delta_C$ |
| 1a | 1.60 m | 20.0 | 1.78 m | 21.0 | 1.91 m | 23.0 |
| 1b | 1.17 m | | 1.27 ddd (16.8, 13.6, 4.5) | | 1.43 ddd (16.7, 12.8, 5.0) | |
| 2a | 2.30 m | 27.6 | 2.48 m | 27.2 | 2.48 m | 26.7 |
| 2b | 2.01[b] | | 2.28 m | | 2.28 m | |
| 3 | 6.73 br d (8.0) | 136.5 | 6.77 br d (7.0) | 137.5 | 6.84 dd (8.0, 2.4) | 137.6 |
| 4 | | 140.0 | | 138.7 | | 135.8 |
| 5 | | 45.7 | | 45.7 | | 46.0 |
| 6a | 2.42 dd (14.0, 2.0) | 35.9 | 1.91 ddd (16.5, 12.8, 5.0) | 30.7 | 2.52 dd (13.5, 8.3) | 40.6 |
| 6b | 1.30 dd (15.0, 4.0) | | 1.49 ddd (16.5, 12.0, 3.8) | | 1.05 dd (13.5, 9.0) | |
| 7a | 4.28 br dd (6.2, 3.7) | 78.7 | 1.93 m | 31.4 | 5.13 t (9.0) | 63.0 |
| 7b | | | 1.70 br d (12.8) | | | |
| 8 | 2.46 dd (7.0, 4.3) | 41.5 | | 85.0 | | 33.0 |
| 9 | | 40.0 | | 47.0 | | 41.0 |
| 10 | 2.04[b] | 40.6 | 2.03[b] | 45.6 | 1.68 dd (13.5, 3.2) | 49.6 |
| 11a | 2.00[b] | 45.6 | 2.10 br t (12.0) | 37.5 | 2.77 d (5.0) | 38.7 |
| 11b | 1.75 dd (15.0, 4.7) | | 2.02[b] | | | |
| 12 | 4.73 dd (8.0, 3.6) | 63.2 | 4.31 dd (11.0, 6.0) | 77.1 | 5.70 br d (5.0) | 74.7 |
| 13 | | 131.5 | | 80.5 | | 123.5 |
| 14 | 6.52 br s | 109.0 | 3.86 d (4.0) | 77.8 | 6.55 s | 109.6 |
| 15 | 7.51 br s | 144.0 | 4.90 d (4.0) | 112.0 | 7.58 br s | 145.0 |
| 16 | 7.52 s | 139.5 | 4.80[b] | 109.8 | 7.62 s | 140.5 |
| 17 | 1.23 d (6.0) | 12.5 | 1.22 s | 25.8 | | 177.0 |
| 18 | | 172.0 | | 171.0 | | 171.0 |
| 19a | 5.52 d (8.0) | 73.4 | 4.46 d (8.0) | 71.3 | 4.13 s | 70.4 |
| 19b | 3.95 d (8.0) | | 4.03 d (8.0) | | | |
| 20 | 0.82 s | 18.0 | 0.87 s | 16.2 | 0.90 s | 13.0 |
| OMe at C-15 | | | 3.46 s | 55.2 | | |
| OMe at C-16 | | | 3.38 s | 54.7 | | |
| 1' | 4.46 d (8.3) | 101.9 | | | | |
| 2' | 4.14 d (8.3) | 77.5 | | | | |
| 3' | | 207.9 | | | | |
| 4' | 4.25 d (9.0) | 73.5 | | | | |
| 5' | 3.33[b] | 77.5 | | | | |
| 6'a | 3.98 dd (12.0, 3.0) | 62.2 | | | | |
| 6'b | 3.83 dd (12.0, 4.5) | | | | | |

[a] *J* values are in parentheses and reported in Hz; chemical shifts are given in ppm; assignments were confirmed by DQF-COSY, 1D-TOCSY, HSQC, and HMBC experiments.

[b] overlapped signal.

**Table 2**

LDH5 and MAGL inhibition potencies for compounds **1-4**, galloflavin, and CL6a.

| Compound | $IC_{50}$ (μM) | |
|---|---|---|
| | LDH5 | MAGL |
| **1** | > 200 | > 200 |
| **2** | > 200 | > 200 |
| **3** | > 200 | > 200 |
| **4** | > 200 | 46.8 ± 5.0 |
| galloflavin[a] | 103.1 ± 5.4 | - |
| CL6a[b] | - | 11.7 ± 2.2 |

Data were reported as means ± SD of three independent measurements.

[a] positive control for LDH5.

[b] positive control for MAGL.